American Mineralogist, Volume 85, pages 194–205, 2000

In-situ study of the $R\bar{3}$ to $R\bar{3}c$ phase transition in the ilmenite-hematite solid solution using time-of-flight neutron powder diffraction

RICHARD J. HARRISON,[1,*] SIMON A.T. REDFERN,[2] AND RON I. SMITH[3]

[1]Institut für Mineralogie, Universität Münster, Corrensstrasse 24, 48149 Münster, Germany
[2]Department of Earth Sciences, University of Cambridge, Downing Street, Cambridge CB2 3EQ, U.K.
[3]ISIS Facility, CLRC Rutherford Appleton Laboratory, Chilton, Didcot OX11 0QX, U.K.

ABSTRACT

The $R\bar{3}$ to $R\bar{3}c$ cation ordering phase transition in the ilmenite ($FeTiO_3$) – hematite (Fe_2O_3) solid solution has been investigated using in-situ time-of-flight neutron powder diffraction. Four synthetic samples of the solid solution containing 70, 80, 90, and 100% $FeTiO_3$ (ilm70, ilm80, ilm90, and ilm100, respectively) were heated under vacuum to a maximum of 1350 °C. Powder diffraction patterns were collected at several temperatures on heating and cooling, with a Rietveld refinement performed in each case. Samples ilm80, ilm90, and ilm100 were fully ordered after quenching from the synthesis temperature to room temperature. Sample ilm70 had a higher degree of quenched in disorder, which is the result of chemical heterogeneities produced during quenching and subsequent heating in the neutron experiments. The degree of order in all samples decreased smoothly at high temperatures, with second-order transitions to the $R\bar{3}c$ phase being observed at 1000, 1175, and 1325 °C in ilm70, ilm80, and ilm90, respectively. The transition temperature in ilm100 was higher than the maximum temperature reached in the neutron experiments, and is estimated as ~1400 °C. The character of the transition is typical of that predicted by three-dimensional Ising models and appears to become more first-order in character with increasing Ti-content. The temperature-dependence of the cell parameters reveals that components of the spontaneous strain tensor, e_{11} and e_{33}, are negative and positive, respectively. Little volume strain is associated with long-range ordering. A small negative volume strain due to short-range ordering within the $R\bar{3}c$ phase is identified. The variations in cell parameters and cation-cation distances can be understood in terms of the competing effects of long- and short-range ordering as a function of temperature and composition.

INTRODUCTION

The rhombohedral oxide solid solution between ilmenite ($FeTiO_3$) and hematite (Fe_2O_3) is significant to both petrology and paleomagnetism. The equilibrium between coexisting rhombohedral and spinel oxides in the Fe-Ti-O system is commonly used to determine the temperature and oxygen fugacity at which a natural assemblage was formed (Buddington and Lindsley 1964). Members of the $(FeTiO_3)_x(Fe_2O_3)_{1-x}$ solid solution with compositions $0.5 < x < 0.75$ have large saturation magnetizations and contribute significantly to the paleomagnetic record (Banerjee 1991). Often such material is observed to acquire self-reversed remnant magnetization (Nord and Lawson 1989, 1992). In all cases, the high-temperature $R\bar{3}$ to $R\bar{3}c$ cation ordering transition plays a crucial role in determining the thermodynamic and magnetic properties. This transition involves the partitioning of Ti and Fe cations between alternating (001) layers of the oxygen sublattice. Above the transition temperature (T_c) the cations are distributed randomly over all (001) layers. Below T_c the cations order to form Fe-rich A-layers and Ti-rich B-layers.

The existence of a second-order phase transition in the ilmenite-hematite system was first demonstrated from measurements of saturation magnetization on quenched samples with compositions $0.53 < x < 0.74$ (Ishikawa 1958 and 1962; Ishikawa and Akimoto 1957; Ishikawa and Syono 1963). Over this range in composition, the solid solution adopts a ferrimagnetic structure, in which the magnetic moments on the A-layers are aligned anti-parallel to those on the B-layers. In the ordered phase, more Fe is on the A-layers than on the B-layers, leading to a net ferrimagnetic moment. In the disordered phase, equal amounts of Fe on the A- and B-layers leads to a canted antiferromagnetic structure with almost zero magnetic moment. Hence, one can derive a simple relationship between the net saturation magnetization and the distribution of Fe between the layers (the so-called quench-magetization technique).

To date this has been the most common technique for studying the phase transition. Its application, however, has several shortcomings. First, it is necessary to make an assumption about the distribution of Fe^{2+} and Fe^{3+} between the A- and B-layers. It is normally argued on the basis of electrostatic energy mini-

*E-mail: harrisr@nwz.uni-muenster.de

mization that Fe^{3+} is equally distributed between the layers (Brown et al. 1993). This has never been demonstrated directly, however, despite detailed attempts to do so using Mössbauer spectroscopy (Warner et al. 1972). Second, the magnetic properties of quenched material are affected by the presence of transition-induced twin-domain boundaries (Nord and Lawson 1989). The twin domains are ordered and have a large magnetization. The twin boundaries, however, are disordered and have a small magnetization. The net magnetization, therefore, is a function of the total volume of twin domain boundary, which, in turn, is a complex function of the thermal history of the sample. The third and most serious shortcoming of the quench-magnetization technique is that, for compositions more Ti-rich than $x = 0.6$, it is not possible to quench-in the high-temperature disordered phase (Brown et al. 1993). For $x > 0.6$, the kinetics of Fe-Ti exchange are sufficiently rapid to allow some degree of cation re-ordering to occur during the quench. In fact, for compositions close to pure $FeTiO_3$, samples can reorder fully on quenching. Consequently, data are presently lacking on equilibrium cation distributions in the solid solution for compositions $0.7 < x < 1$.

These problems can be overcome by determining the cation distribution directly using in-situ diffraction techniques. X-ray diffraction is not suitable because of the small difference between the atomic scattering factors of Fe and Ti. Neutron diffraction, however, is ideal because the scattering length for Fe is large and positive ($b = 9.54$ fm) whereas that for Ti is small and negative ($b = -3.44$ fm) (Shirane et al. 1959 and 1962). Previous studies on oxidation-sensitive minerals have shown that time-of-flight neutron powder diffraction can be used effectively at high temperatures, without changing the oxidation state of the sample (Harrison et al. 1998 and 1999; Redfern et al. 1996; Grguric et al. 1999). This is possible because the experiments are performed under high vacuum in the presence of a buffer. It is possible to obtain high-quality diffraction information at *d*-spacings as low as 0.4 Å. Hence, structural parameters can be determined from the powder diffraction patterns using Rietveld refinement to a precision which, in many cases, rivals that of single-crystal structure refinements.

Here we present an in-situ time-of-flight neutron powder diffraction study of the $(FeTiO_3)_x(Fe_2O_3)_{1-x}$ solid solution with compositions $x = 0.7$, 0.8, 0.9, and 1.0. The measurements provide insight into the equilibrium behavior of this system over this compositional range and allow us to observe simultaneously the changes in degree of order, spontaneous strain, and the cation-cation distances as a function of temperature. A qualitative interpretation of the observations is provided in terms of long- and short-range ordering processes. A full thermodynamic analysis of the results is the subject of a separate paper.

CRYSTAL STRUCTURE

All samples studied here adopt the ordered ilmenite structure at room temperature, with space group $R\bar{3}$. The oxygen anions occupy the general positions, forming a distorted hexagonal-close-packed arrangement. Cations occupy 2/3 of the octahedral interstices. A-site cations occupy the sixfold *c*-Wyckoff site (0, 0, *z*; symmetry 3) with $z \approx 0.35$. B-site cations occupy a second *c*-Wyckoff site with $z \approx 0.15$. Conventionally, it is assumed that Fe orders onto the A-sites and Ti onto the B-sites. The A- and B-site cations form alternating hexagonal layers parallel to (001). Figure 1a illustrates the cation arrangement within one (001) layer. The hexagonal rings are puckered so that adjacent cations are displaced slightly up and down the [001] axis (Fig. 1b). Figure 1c is a perspective view of the nearest-neighbor cation-cation relationships. The oxygen co-ordination octahedra share faces across the nearest-neighbor interlayer join (A-B) and share edges across the nearest-neighbor intralayer join (A-A and B-B).

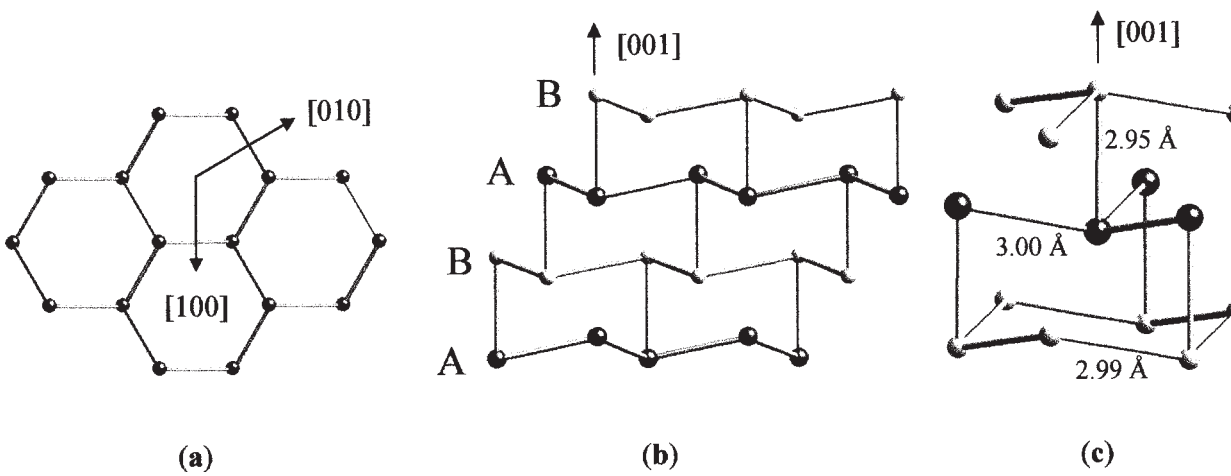

FIGURE 1. Topology of the ordered ilmenite structure, showing Fe (dark) and Ti (light) cation positions only. (**a**) View of a single A-cation layer down the [001] axis. (**b**) View of the ordered A- and B-cation layers down the [100] axis. (**c**) Definition of nearest-neighbor A-A, B-B, and A-B cation-cation distances. Distances quoted are for ordered ilmenite at room temperature (Table 3). The structure is drawn without the oxygen sublattice and bonds are drawn to represent the nearest-neighbor cation-cation distances.

In the disordered phase, the Fe and Ti cations are randomly distributed over all (001) layers. In this case the A- and B-layers are symmetrically equivalent (related to each other via a *c*-glide plane) and the space-group symmetry is $R\bar{3}c$. The oxygen anions now occupy the 18-fold *e*-Wyckoff site (x, 0, 1/4; symmetry 2) and the cations occupy the 12-fold *c*-Wyckoff site (0, 0, z; symmetry 3). The presence of the *c*-glide plane in the disordered phase leads to the disappearance of reflections of the type $h\bar{h}0l$, $l = 2n + 1$ from the diffraction patterns.

Experimental details

Sample synthesis

The samples were synthesized from the oxides Fe_2O_3 and TiO_2 under controlled oxygen fugacity. Stoichiometric mixes of up to 8 g were weighed to yield bulk compositions containing 70, 80, 90, and 100% $FeTiO_3$ (samples ilm70, ilm80, ilm90, and ilm100, respectively) and homogenized by grinding under acetone using an agate mortar and pestle. Each oxide mix was then pressed into several pellets using a 13 mm diameter die. A series of preliminary annealing experiments were performed to determine the precise oxygen fugacity conditions required to produce stoichiometric material at each bulk composition. Small chips from the sample pellets were suspended in a vertical-tube gas-mixing furnace using two loops of Pt wire and annealed in a controlled mixture of CO_2 and CO gases at 1300 °C for 24 hours, following Nafziger et al. (1971). Stable and precise control of the gas mixture was obtained using two Tylan-General electronic gas-flow controllers, which were calibrated specifically for CO_2 and CO. After each annealing experiment the sample chip was quenched directly from the furnace into water and examined using a Philips X-ray diffractometer (Cu$K\alpha$ radiation). If the chosen ratio of CO_2 to CO was too high (oxidizing) then traces of the pseudobrookite-ferripseudobrookite solid solution appeared clearly in the diffraction pattern (Waychunas 1991). If the chosen ratio was too small (reducing) then traces of the magnetite-ulvöspinel solid solution appeared. A small range of gas ratios for each bulk composition gave rise to single-phase diffraction patterns with sharp peaks corresponding to the rhombohedral phase only. The center of this range was chosen for the main synthesis experiments (Table 1).

The main synthesis experiments were performed by annealing several pressed pellets of the stoichiometric oxide mix for 24 hours under the conditions given in Table 1. After quenching into water, a small amount from each pellet was ground with Si and examined using powder XRD over the range $22° < 2\theta < 89°$. The peak positions were determined by peak fitting and then corrected using a cubic spline fit to the six observable Si peaks. The lattice parameters (Table 1) were determined using the least-squares program *UnitCell* (Holland and Redfern 1997). Good agreement was observed between the unit cell volumes of the synthetic samples and the calibration given by Brown et al. (1993) based on their own experiments and those of Lindsley (1965). After XRD analysis, the samples were reground under acetone, pressed into pellets and annealed for a further 24 hours under the same conditions. The final product was a stack of sintered pellets of 13 mm diameter and between 30 and 40 mm height for each bulk composition. These pellet stacks were used directly in the neutron diffraction experiments.

Neutron diffraction procedures

The neutron powder diffraction data were collected using the high-intensity POLARIS time-of-flight diffractometer at the ISIS spallation neutron source (Rutherford Appleton Laboratory, U.K.). Diffracted intensity was measured using fixed-angle detectors located at a scattering angle of $2\theta = 90°$. The samples were loaded into a high-temperature Ta furnace, which was evacuated to a pressure of 4×10^{-5} mbar to prevent both the Ta elements and the sample from oxidizing during the experiment. The vacuum improved as the furnace de-gassed at high temperatures, reaching a minimum pressure of 1.6×10^{-6} mbar. No evidence of either oxidation or reduction of the sample was detected during the experiments. This observation is consistent with our previous experience using Fe-bearing samples in this equipment, and can be attributed to the low oxygen fugacity imposed by the Ta furnace (essentially at Ta-TaO).

Experiments on ilm70 were performed by suspending the stack of pellets in a basket of 0.5 mm diameter Pt wire. Kinks introduced into the Pt during fabrication of the basket severely weakened the wire at high temperatures. In this case the basket broke during the data collection at 1200 °C, preventing us from performing a satisfactory structure refinement at this temperature and obtaining data during cooling. Subsequent experiments were performed by suspending the sample pellets in a basket of 0.25 mm diameter Ir wire. The Ir wire had the advantage of having a large critical resolved sheer stress, high melting point and a low reactivity. No scattering from Ir was detectable in the diffraction patterns and no visible reaction with the sample occurred up to the highest temperature studied.

Neutron diffraction patterns were collected at several temperatures during heating. The temperature was controlled and monitored using type K thermocouples, placed just above the sample pellet stack. The sample was heated to the desired temperature and left to thermally equilibrate for 5 minutes. Neutron data were then acquired over a period of 50 minutes. The maximum temperatures reached were 1200, 1325, 1350, and 1325 °C for the compositions ilm70, ilm80, ilm90, and ilm100,

Table 1. Synthesis conditions and lattice parameters for ilmenite-hematite starting material

Composition (x)	Temperature (°C)	Volume ratio (CO_2/CO)	f_{O_2}†	a (Å)	c (Å)	V (Å^3)
0.7	1300	0.990	–5.75	5.0731(7)	13.943(4)	310.7(2)
0.8	1300	0.976	–6.50	5.0786(4)	13.985(3)	312.37(9)
0.9	1300	0.928	–7.50	5.0828(7)	14.033(3)	313.97(13)
1.0	1300	0.600	–9.40	5.08795(60)	14.088(3)	315.8(1)

† Oxygen fugacity determined from tabulated values in Deines et al. (1974).

respectively. After heating to 1350 °C, the sample of ilm90 showed signs of flow at the edges of the pellets, suggesting that this temperature was close to the melting point for that bulk composition. A small number of diffraction patterns were collected during cooling of the ilm80, ilm90, and ilm100 samples.

The crystal structures were refined assuming ideally stoichiometric total site occupancies using the GSAS Rietveld refinement software (Larson and Von Dreele 1994). All diffraction patterns displaying ordering reflections of the type $h\bar{h}0l$, $l = 2n + 1$ were refined using the low-symmetry space-group $R\bar{3}$. Diffraction patterns with no visible ordering reflections were refined initially using the low-symmetry space-group. In these cases, however, convergence could not be achieved, and the high-symmetry space-group $R\bar{3}c$ was used. The background was modeled using a 6th-order Chebyshev polynomial. The crystallographic variables were the unit-cell parameters (a and c), the z-coordinates of the two cation sites (z_A and z_B), the x-, y-, and z-coordinates of the oxygen atom (x , y_o, and z_o), the A-site Ti occupancy (X^A_{Ti}) and the isotropic cation and oxygen displacement parameters (U_c and U_o). It was not possible to refine the displacement parameters for the A- and B-sites independently because, at certain stoichiometries and degrees of order, the total scattering from the B-site went through zero. To overcome this problem, the displacement parameters for both sites were constrained to be equal. Peak-shape parameters and a correction parameter for the wavelength-specific absorption of neutrons by the sample were also refined. The diffraction patterns collected for ilm70 contained small contributions from Pt. This was accounted for by including Pt as a second phase in the Rietveld refinement. For this phase the unit-cell parameter, the temperature factor, peak profiles, and the phase fraction were refined. Except for ilm70 at room temperature, the samples were paramagnetic and there was no contribution to the diffraction patterns from magnetic scattering. An attempt to refine simultaneously the crystal and magnetic structure of ilm70 at room temperature failed due to high correlation between the magnetic and cation order parameters.

The results of the structure refinements are listed in Table 2 (selected inter- and intralayer cation-cation distances are listed in Table 3).[1] Because the neutron diffraction experiments were performed without an internal calibration standard, the absolute values of the cell parameters are subject to systematic error due to the uncertainty of the sample position within the furnace. For the purposes of comparing the cell parameters from different samples, the neutron diffraction results are calibrated relative to the known room temperature cell parameters obtained with an internal standard (Table 1).

[1]For a copy of Tables 2 and 3, document item AM-00-033, contact the Business Office of the Mineralogical Society of America (see inside front cover of recent issue) for price information. Deposit items may also be available on the American Mineralogist web site (http://www.minsocam.org or current web address).

RESULTS

In-situ cation distributions as a function of T and x

In discussing the changes in cation distribution which occur as a function of temperature, T, and composition, x, we define a long-range interlayer order parameter, Q, as follows:

$$Q = \frac{\left(X^B_{Ti} - X^A_{Ti}\right)}{\left(X^B_{Ti} + X^A_{Ti}\right)} \quad (1)$$

The order parameter is $Q = 0$ in the fully disordered state (with Fe and Ti statistically distributed between the A- and B-layers) whereas $Q = 1$ in the fully ordered state (with the A-layer fully occupied by Fe and all available Ti on the B-layer).

The value of Q (Table 1, Fig. 2) at room temperature represents the degree of order quenched-in after synthesis. In ilm80, ilm90, and ilm100 the quenched starting material is almost fully ordered, with $Q = 0.98$ in all three cases. The ilm70 sample has a higher degree of quenched-in disorder, with $Q = 0.82$ estimated from quench-magnetization measurements and $Q = 0.79$ being measured directly using neutron diffraction at 200 °C. On heating from room temperature to 400 °C, the degree of order increases in all four samples, reaching a maximum value of $Q = 0.85$ in ilm70 and $Q = 0.99$ in ilm80, ilm90 and ilm100. This behavior is referred to as "order parameter relaxation", and is often observed in in-situ experiments on quenched starting material (Harrison et al. 1998; Redfern et al. 1996 and 1999). Relaxation occurs because the quenched-in degree of order is lower than the equilibrium degree of order, hence there is a driving force for ordering as the sample is heated. Ordering is observed when the temperature is high enough to allow cation exchange to occur on the timescale of the measurement. At some temperature (400 °C in this case), the kinetic path intersects the equilibrium path and the sample begins to disorder. We conclude, therefore, that data points measured at 400 °C and above represent equilibrium behavior. It is surprising to observe that the equilibrium degree of order in ilm70 at this temperature is significantly less than for the other three samples. This low value of Q may be due to the presence of chemical heterogeneities which develop on heating the sample below the solvus. Evidence to support this suggestion will be described in a later section.

Above 400 °C, the degree of order decreases smoothly in all four samples, with transitions to the high-temperature $R\bar{3}c$ phase occurring at 1000, 1175, and 1325 °C in ilm70, ilm80, and ilm90, respectively. A phase transition was not observed in ilm100 because the transition temperature was greater than the maximum temperature reached (1325 °C in this case). However, a significant amount of disorder is observed above 1100 °C, with a minimum value of $Q = 0.732$ being reached at 1325 °C. The observation that little disorder occurs below 1100 °C is consistent with the in-situ single-crystal X-ray diffraction experiments of Wechsler and Prewitt (1984), in which no disorder was observed in a synthetic sample of $FeTiO_3$ at 1050 °C.

The ordering behavior in ilm80, ilm90, and ilm100 appears to be fully reversible, confirming that the samples remained stoichiometric for the duration of the heating experiments and that the high-temperature structures represent equilibrium.

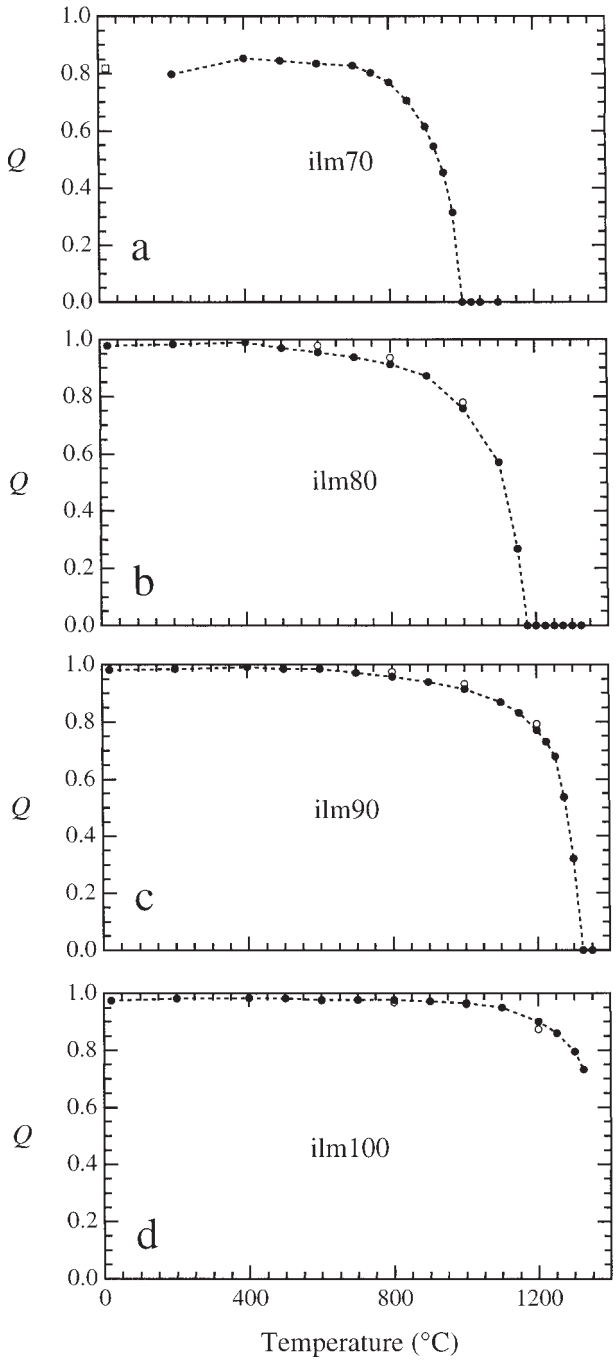

FIGURE 2. Cation order parameter, *Q*, as a function of temperature (°C) for synthetic samples of (**a**) ilm70, (**b**) ilm80, (**c**) ilm90, and (**d**) ilm100. Solid circles are values measured during heating of the quenched starting material, open circles are values measured on subsequent cooling. The open square in (**a**) is an estimate of the quenched-in degree of order in the starting material using the quench-magnetization technique. In all cases the estimated standard deviation in *Q* is smaller than the size of the symbols.

Cell parameters as a function of *T* and *x*

Significant changes in both *a* and *c* correlate with the phase transition (Table 2, Fig. 3). Such changes are usually described by the spontaneous strain tensor, e_{ij}, which relates the cell parameters of the low-symmetry phase to those of the hypothetical high-symmetry phase at the temperature of interest (Carpenter et al. 1998). The diagonal components of e_{ij} describe extentions or contractions along the three crystallographic axes. The off-diagonal components describe shear strains. In the case of the $R\bar{3}c$ to $R\bar{3}$ transition, where there is no change in crystal system, the only non-zero components are $e_{11} = e_{22} \neq e_{33}$, where:

$$e_{11} = \frac{a - a_0}{a_0} \; ; \; e_{33} = \frac{c - c_0}{c_0} \qquad (2)$$

In addition, a change in volume may also be associated with the phase transition, described by the volume strain, e_v, where:

$$e_v = \frac{V - V_0}{V_0} \qquad (3)$$

The variables a_0, c_0, and V_0 are the cell parameters and volumes of the high-symmetry phase extrapolated from above T_c to the temperature of interest. This extrapolation removes the effects of intrinsic thermal expansion (i.e., that which occurs at a constant degree of long- and short-range order), so that e_{ij} and e_v refer to the excess strains due exclusively to the phase transition.

Estimating a_0, c_0, and V_0 is made difficult by two factors. First, the temperature range over which data for the high-symmetry phase have been obtained is limited in ilm90, and non-existent in ilm100. Second, the thermal expansion observed above T_c in ilm70 and ilm80 is significantly non-linear. One possible cause of this non-linearity is the temperature-dependent short-range ordering of cations within the $R\bar{3}c$ phase. For these reasons, we chose to constrain the intrinsic thermal expansion in this system using the cell parameter data measured below 600 °C, where only small changes in the degree of long-range order are observed (Fig. 2) and the degree of short-range order is expected to be small. The estimated variation in a_0, c_0, and V_0 as a function of temperature is shown by the dashed lines in Figure 3. The slopes, da_0/dT, dc_0/dT, and dV_0/dT, were obtained by fitting straight lines to the cell parameter data below 600 °C. The intercepts were then chosen so that a_0, c_0, and V_0 passed through the observed value at $T = T_c$. Because T_c was never reached in ilm100, the values of a_0, c_0, and V_0 for this composition are not defined. The dashed lines in Figure 3 represent possible values based on the trends defined by the other three samples.

In Figure 3a, e_{11} is negative and the magnitude of e_{11} increases with increasing Ti-content. The changes in *a* occur smoothly over a large temperature range and there is no sharp change in trend at $T = T_c$ in any of the samples. In Figure 3b, e_{33} is positive and the magnitude of e_{33} also increases with increasing Ti-content. In ilm70, e_{33} is relatively small and *c* varies smoothly through the transition. In ilm80 and ilm90, e_{33} is larger and the decrease in *c* occurs abruptly at the phase transition. In Figure 3c, a comparatively small volume strain is associated with the transition, because the negative e_{11} strain is compensated by the positive e_{33} strain ($e_v \approx 2e_{11} + e_{33}$). In ilm70 essentially no volume strain is associated with long-range ordering.

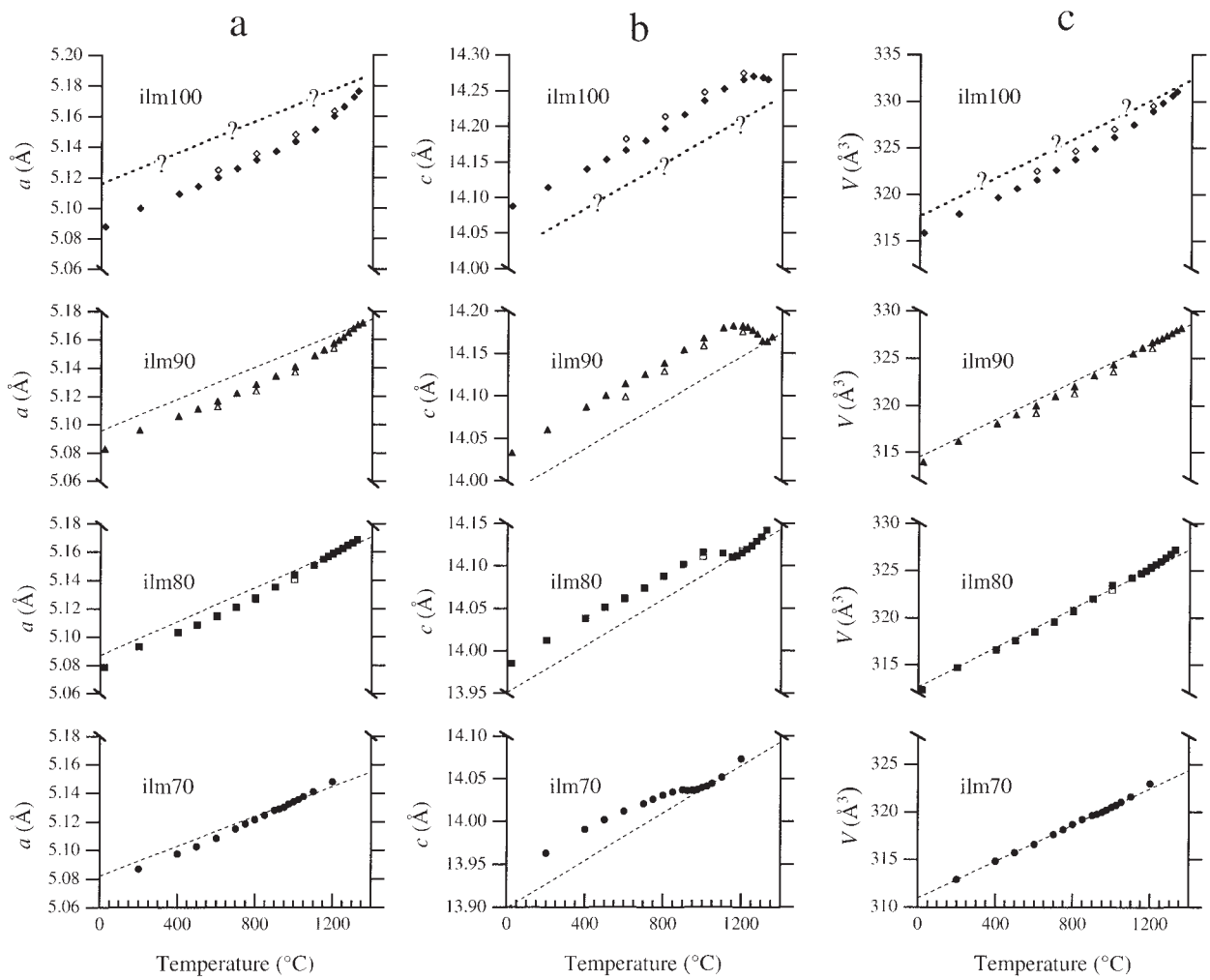

FIGURE 3. Variation in the cell parameters (**a**) a, (**b**) c, and (**c**) V as a function of temperature (°C) for ilm70 (circles), ilm80 (squares), ilm90 (triangles), and ilm100 (diamonds). Solid symbols are values measured during heating of the quenched starting material, open symbols are values measured on subsequent cooling. Dashed lines are the estimated variation in a_0, c_0, and V_0 as a function of temperature (i.e., the intrinsic thermal expansion of the high symmetry phase). Where not shown, the error bars are approximately equal to the size of the symbols.

In ilm80, ilm90, and ilm100, e_v is small and negative, with the magnitude of e_v increasing with increasing Ti-content.

The magnitude of all spontaneous strains associated with ordering in these samples is relatively small. This is consistent with the observations of Nord and Lawson (1989), who studied the twin-domain microstructure associated with the order-disorder transition. The twin boundaries are not strongly aligned and have wavy surfaces, as is expected if strain does not control their orientation. Furthermore, the small spontaneous strain on ordering hints that the length scale of the ordering interactions may not be long-range. Generally, systems that display large strains on ordering tend to behave according to mean field models, as the strain mediates long-range correlations, whereas systems with weak strain interactions tend to show bigger deviations from mean-field behavior.

In ilm70 and ilm80 at $T > T_c$, a, c, and V vary non-linearly with temperature and lie significantly above the intrinsic thermal expansion baseline. This behavior may indicate the presence of a volume strain associated with short-range ordering in the $R\bar{3}c$ phase. The degree of short-range order is expected to decrease smoothly at temperatures above T_c. In this case, the sign of the volume strain would be negative, because V is observed to increase as the degree of short-range order decreases. An alternative explanation is that the intrinsic thermal expansion has a significant positive curvature over the large temperature range of the measurements. Although we cannot rule this out, it will be argued later that the presence of a negative volume strain due to short-range ordering provides an explanation for the contrasting temperature-dependence of e_{11} and e_{33} in ilm80 and ilm90.

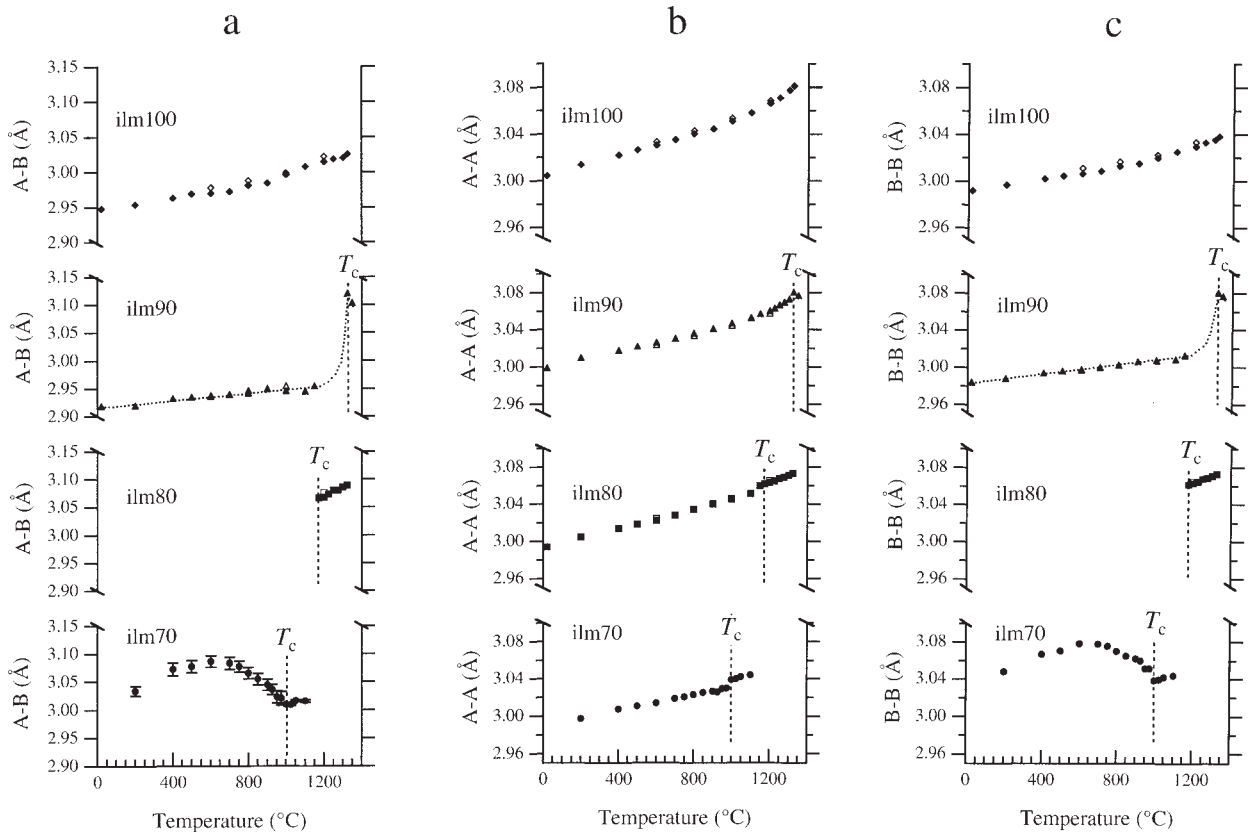

FIGURE 4. Variation in the nearest-neighbor cation-cation distances for (**a**) A-B interlayer pairs, (**b**) A-A intralayer pairs, and (**c**) B-B intralayer pairs as a function of temperature (°C) for ilm70 (circles), ilm80 (squares), ilm90 (triangles), and ilm100 (diamonds). Solid symbols are values measured during heating of the quenched starting material, open symbols are values measured on subsequent cooling. Dashed lines show the position of T_c for the long-range $R\bar{3}$ to $R\bar{3}c$ transition. See Figure 1c for definitions.

Cation-cation distances as a function of *T* and *x*

For certain bulk compositions and degrees of cation order the ratio of Fe to Ti on the B-layer is such that the negative scattering length of Ti just balances the positive scattering length of Fe. In this case the total scattering length at the B-site is zero and the coordinates of this site become poorly determined in the structure refinement, resulting in cation-cation distances which may be unphysical. Empirically we chose to ignore cation-cation distances when the magnitude of the B-site scattering length was less than 1 fm, because structures determined with smaller scattering lengths did not correspond to the topology of the ilmenite structure. This problem is most severe in ilm80, because the magnitude of the B-site scattering length is less than 1 fm over the temperature range 20 °C < T < 1100 °C in this sample. In ilm90 the problem occurs over the temperature range 1150 °C < T < 1300 °C. In ilm70 and ilm100 the magnitude of the scattering length is greater than 1 fm for all temperatures studied. Only those distances calculated with B-site scattering lengths greater than 1 fm are reported in Table 3.

In ilm70 at 200 °C, the A-B interlayer distance is greater than the A-A intralayer distance and approximately equal to the B-B intralayer distance (Fig. 4). On heating from 200 °C to 600 °C, the A-B and B-B distances increase at a rate which appears to be much faster than the rate of thermal expansion in ilm90 and ilm100 (Figs. 4a and 4c), whereas the A-A distance increases at a rate similar to that observed in ilm80, ilm90, and ilm100 (Fig. 4b). The A-B and B-B distances reach a maximum length at 600 °C and thereafter begin to decrease smoothly with increasing temperature. A further change in trend occurs at the transition temperature (T_c = 1000 °C), above which the A-B and B-B distances increase with increasing temperature once more. The transition is accompanied by a small but rapid increase in the A-A distance.

In ilm90 the room-temperature A-B distance is smaller than both the A-A and B-B intralayer distances (Fig. 4). This is also observed in ilm100, and is consistent with the single-crystal X-ray structure refinement of ilm100 by Wechsler and Prewitt (1984). On heating, the A-B, A-A, and B-B distances increase approximately linearly up to a temperature of around 1150 °C. The A-A distance expands at a much greater rate above 1150 °C, reaching a maximum value at the transition temperature (T_c = 1325 °C). The single data point measured above T_c has a significantly lower value. The A-B and B-B distances measured at 1325 and 1350 °C are much larger than those measured below 1150 °C,

implying a sharp increase in these distances is associated with the transition (shown by the dotted lines in Figs. 4a and 4c). In both cases the cation-cation distance measured at 1350 °C is significantly lower than that measured at 1325 °C.

Comparing the available data for all four samples it appears that ilm70 behaves unusually in three respects. First, the A-B and B-B distances in the quenched starting material are much higher than expected; second, the rapid increase in A-B and B-B distances between 20 and 600 °C is not observed in the other samples; and third, the trend of decreasing A-B and B-B distance with increasing temperature above 600 °C is not consistent with the behavior observed in ilm90.

DISCUSSION

T_c as a function of x

The variation in T_c as a function of x is shown in Figure 5 within the context of the phase diagram calculated by Burton (1985) using the cluster variation method (CVM) (Kikuchi 1951). Good agreement between the transition temperatures in this study and those calculated using CVM is observed. Our value of T_c = 1000 °C in ilm70 is in reasonable agreement with the value of 1010 °C reported by Ishikawa (1958) for a sample with x = 0.675 and the value of 1000 °C < T_c < 1050 °C reported by Nord and Lawson (1989) for a sample with x = 0.7. The value of T_c = 1150 °C reported by Ishikawa (1958) for a sample with x = 0.74 appears to lie significantly above the trend defined by this study, however. This difference is due to T_c being determined from in-situ measurements in this study whereas Ishikawa (1958) determined T_c from quenched samples.

Burton (1985) calculated a value of T_c = 1400 °C in ilm100, which places the transition temperature just above the melting point (1367 °C; Fig. 5). We find a value of Q = 0.732 in ilm100 at 1325 °C (Fig. 2d). In ilm90 the order parameter was observed to drop from Q = 0.731 to Q = 0 over a temperature range of 100 °C (Fig. 2c). Given this, and the observation that the transition becomes steeper with increasing Ti-content (see Fig. 6), the observed ordering behavior in ilm100 is entirely consistent with the transition temperature being close to 1400 °C.

Thermodynamic character of the phase transition

The thermodynamic character of the transition can be assessed more clearly by plotting Q as a function of T/T_c (Fig. 6). A value of T_c = 1400 °C was assumed for ilm100, in accord with the arguments above. With the exception of ilm70 at low temperature, all four samples show ordering behavior which lies well above the Bragg-Williams approximation (Fig. 6). In this model the enthalpy of the transition is calculated assuming nearest-neighbor interactions and the entropy of the transition is taken to be the ideal configurational point entropy. This discrepancy reflects the failure of the Bragg-Williams model to account for correlations between neighboring sites (short-range order). Such correlations are accounted for in Ising models, and the observed behavior in this system is typical of that predicted by two- and three-dimensional Ising models (Ross 1991).

The cluster variation method offers an approximate solution to the Ising model in three-dimensions by reducing the lattice to a small set of basic clusters of cation sites which fit together to generate the whole structure. The free energy of the system is formulated in terms of the energy and probability of each cluster configuration and minimized with respect to the long- and short-range order parameters, which describe correlations in cation occupancy throughout the structure. The larger the size of the basic cluster chosen, the closer the model is to the exact solution for the three-dimensional Ising model. Burton (1984, 1985) proposed a model for the ilmenite-hematite solid solution based on the single-prism approximation of the cluster variation method. This model took into account nearest-neighbor interactions between the layers (A-B interactions) and within the layers (A-A and B-B interactions). To reproduce the general topology of the phase diagram with only two interactions, it was necessary to assume that A-B interactions were negative (i.e., Fe-Ti bonds between the layers are favorable) and A-A and B-B interactions were positive (i.e., Fe-Ti bonds within the layers are not favorable). There is excellent qualitative agreement between the CVM calculation and the observed ordering behavior (Fig. 6). Our own preliminary calculations using both CVM and Monte Carlo methods to model the thermodynamics of the order-disorder process show that better agreement can be achieved by including next-nearest-neighbor interactions.

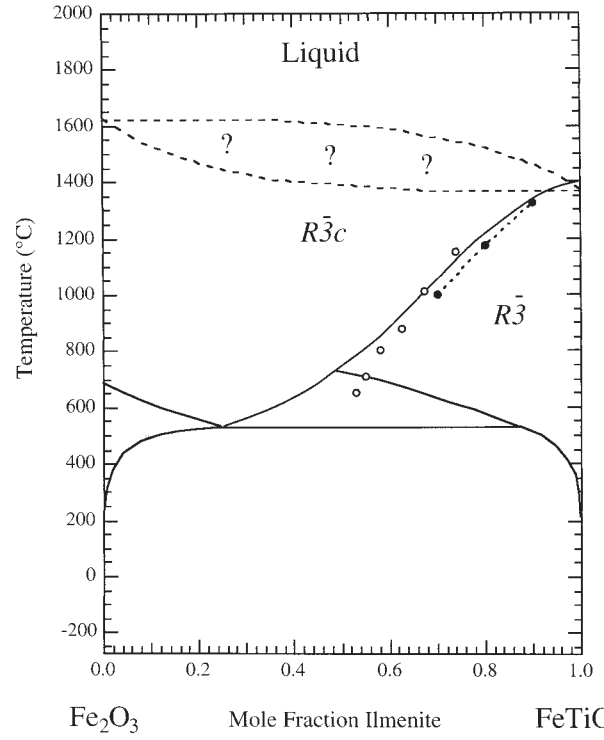

FIGURE 5. Phase relations in the ilmenite-hematite solid solution. Solid lines are the calculated phase boundaries (after Burton 1985). The dashed lines show the possible position of the liquidus and solidus. Solid circles show the transition temperatures of ilm70, ilm80, and ilm90 measured in this study. Open circles are transition temperatures determined by Ishikawa (1958), corrected for errors in composition by Nord and Lawson (1989).

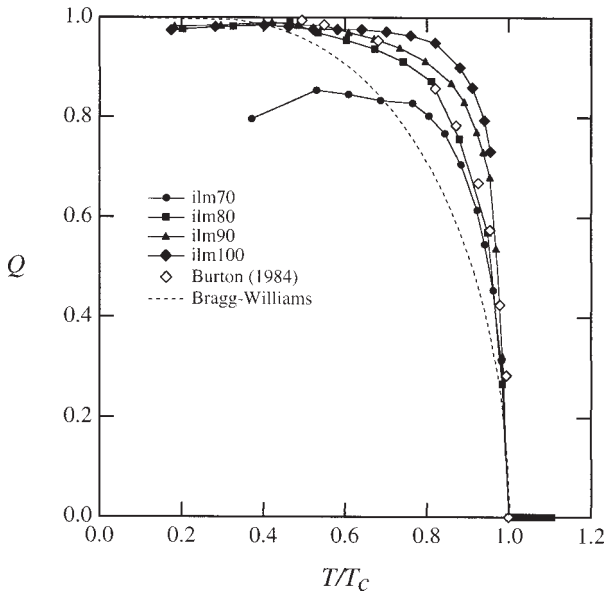

FIGURE 6. Cation order parameter, Q, as a function of reduced temperature, T/T_c. Solid symbols show the results of this study for ilm70 (circles), ilm80 (squares), ilm90 (triangles), and ilm100 (diamonds). Open diamonds show the calculated behavior of ilm100 using CVM (after Burton 1984). The dashed line is the predicted behavior according to the Bragg-Williams model.

The shape of the Q-T curves is a function of the bulk composition, with the transition becoming sharper with increasing Ti-content (Fig. 6). This may indicate a gradual change in transition character from second- to first-order with increasing Ti-content. Any closer investigation of this phenomenon at this stage is difficult due to the low temperature resolution of the data.

Behavior of ilm70 at low temperatures

The degree of order in ilm70 at temperatures below 600 °C is much lower than expected. Ilm80, ilm90, and ilm100 become fully ordered at $T/T_c \approx 0.45$. Given that T_c = 1000 °C in ilm70, one would expect full cation order to be achieved at temperatures below 450 °C in this sample. Instead, a value of $Q \approx 0.85$ is observed. Order parameter relaxation occurs below 400 °C in all four samples and therefore cation distributions measured above 400 °C correspond to equilibrium states. For this reason, it is unlikely that the low degree of order in ilm70 is a kinetic effect caused by failure of the sample to reach equilibrium. It must, therefore, be accounted for in terms of the equilibrium behavior of the sample.

The calculated phase diagram (Fig. 5) illustrates the expected equilibrium behavior of ilm70 at low temperatures. According to Burton (1985), the top of the solvus occurs at a temperature close to 600 °C at this bulk composition. The thermodynamic models of Ghiorso (1990, 1997) predict a similar result. Hence, the ilm70 starting material will experience a driving force for phase separation on quenching below 600 °C. At temperatures between 600 °C and the top of the spinode, phase separation can only proceed via nucleation and growth. This process is associated with a nucleation energy barrier and is unlikely to occur on the timescale of the quench. Ghiorso (1997) places the spinode at a temperature of approximately 475 °C for a bulk composition of ilm70. Below this temperature phase separation can occur by a continuous mechanism of compositional clustering, without the need to nucleate a second phase. Because there is no nucleation energy barrier to overcome, phase separation will occur if the kinetic closure temperature for Fe-Ti exchange is less than 475 °C. The closure temperature is defined as the temperature at which the equilibrium degree of cation order corresponds to the quenched-in degree of order, and gives an upper estimate of the temperature at which Fe-Ti exchange ceases during cooling. From Figure 2 and Table 2 we estimate closure temperatures of 850, 600, and 450 °C in ilm100, ilm90, and ilm80, respectively. Given the trend of decreasing closure temperature with decreasing Ti-content, we conclude that the closure temperature in ilm70 is less than or equal to 450 °C and that some degree of phase separation will have occurred when the starting material was cooled below 475 °C.

The extent of phase separation is expected to be relatively small on quenching, because the temperature interval between the spinode and the kinetic closure temperature is probably quite limited. Exsolution may continue, however, as soon as the sample is heated in the neutron experiments. This means that the data points measured between 200 and 600 °C may be affected by exsolution, whereas those measured above 600 °C (i.e., above the solvus) represent equilibrium behavior in the homogeneous material. This accounts for the change in trend of the A-B and B-B cation-cation distances at 600 °C in Figure 4. It also accounts for the low values of Q observed below 600 °C, as we now show.

One possible model for the Fe and Ti distribution in an exsolved sample of ilm70 is shown in Figure 7. In Figure 7a the sample is homogeneous and fully ordered, with the A-layers occupied by Fe and the B-layers occupied by 0.3 Fe and 0.7 Ti. Figure 7b illustrates the equilibrium state of this material just above the eutectic temperature (525 °C), where the sample consists of an intergrowth of two phases with approximate compositions ilm25 and ilm90 (Fig. 5). The ilm90 phase is fully ordered ($R\bar{3}$), with the A-layer occupied by Fe and the B-layer occupied by 0.1 Fe and 0.9 Ti. The ilm25 phase is disordered ($R\bar{3}c$), with both the A- and B-layers occupied by 0.875 Fe and 0.125 Ti. From mass balance, the ilm90 and ilm25 components constitute 69 and 31% of the sample, respectively. Therefore the average values of X^{A}_{Ti} and X^{B}_{Ti} are 0.03875 and 0.65975, which yields an apparent order parameter of Q = 0.835 (Eq. 1). This compares with the value of Q = 0.85 measured in ilm70 at 500 °C (Fig. 2a, Table 2).

The suggestion that some degree of phase separation occurred in ilm70 on quenching is further supported by the low saturation magnetization observed in this sample (Harrison and Dewhurst, in preparation). The hysteresis loop of the quenched ilm70 starting material was determined at a temperature of 3 K and in a maximum field of 11 T using a vibrating sample magnetometer. A saturation magnetization of M_s = 2.29 μ_B was determined by extrapolating the magnetization curves to infinite field. Assuming that Fe^{3+} is equally distributed over the A- and B-sites (Brown et al. 1993), the theoretical saturation magnetization of fully ordered ilm70 is 2.8 μ_B. The magnetization of

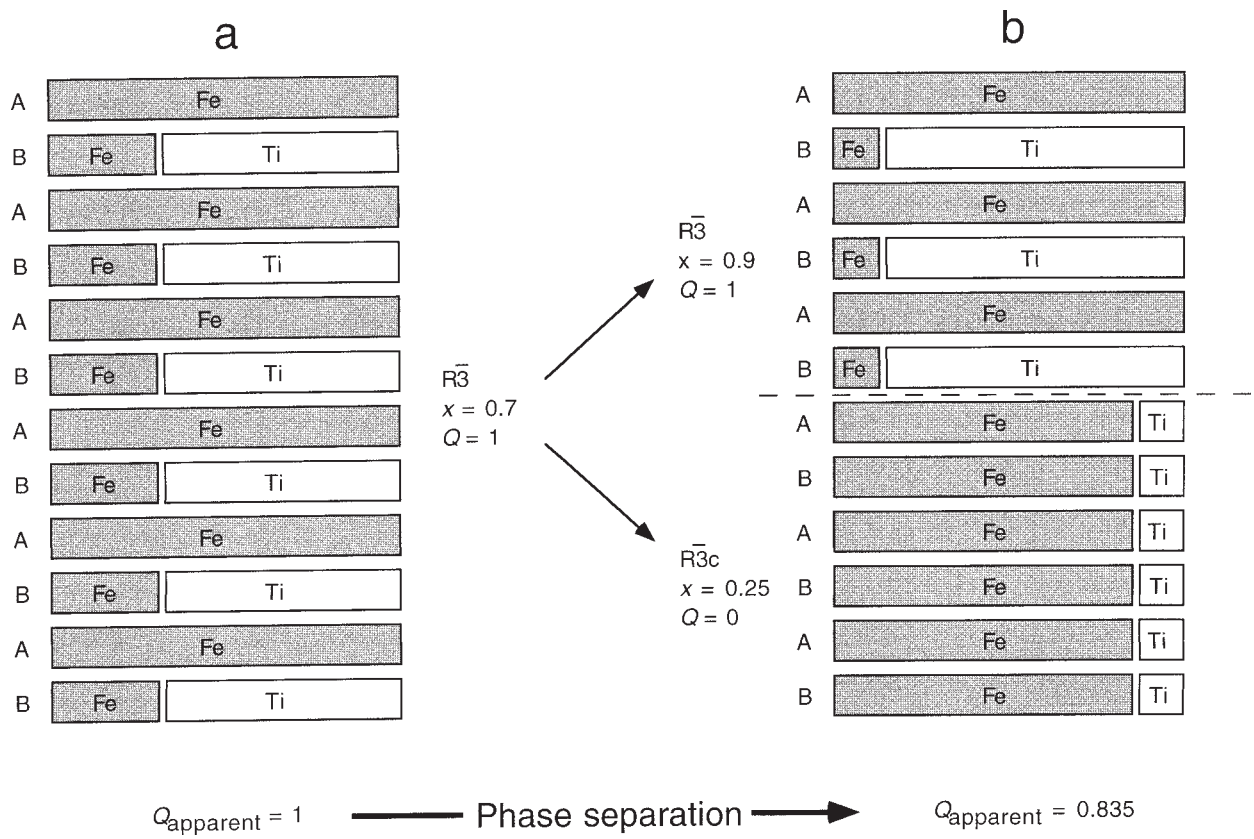

FIGURE 7. Model of the cation distribution in (**a**) homogeneous ordered ilm70 and (**b**) heterogeneous ilm70 consisting of a mixture of ordered ilm90 and disordered ilm25. Shaded boxes represent the relative proportions of Fe (gray) and Ti (white) on the A and B layers.

an exsolved sample would be lower than this because the disordered component of the intergrowth is antiferromagnetic (i.e., has no net magnetic moment). For example, the model presented in Figure 7b has a theoretical magnetization of 2.49 μ_B.

Transition-induced domain boundaries might also play a role in the low-temperature behavior of ilm70. Nord and Lawson (1989) demonstrated that ilm70 quenched from 1300 °C contains twin domains with a diameter of approximately 700 Å. Adjacent domains are in antiphase with respect to their Fe and Ti occupancies, so that Q varies from negative to positive across a domain boundary. The domain boundaries are disordered and are thought to be enriched in Fe relative to the domains (Nord and Lawson 1989 and 1992). Such boundaries might therefore act as nuclei for the disordered Fe-rich phase on cooling below the solvus. In this case, exsolution could proceed immediately below 600 °C in ilm70 by growth of the domain boundaries, hence increasing the temperature interval over which exsolution is kinetically feasible and enhancing the degree of chemical heterogeneity. The volume fraction of domain boundary in ilm80 quenched from 1300 °C is much lower than in ilm70, and no domain boundaries are observed in ilm90 and ilm100 quenched from this temperature (Nord and Lawson 1989). This, together with the spinode lying below the closure temperature at these compositions, explains why no exsolution was observed in the other three samples.

Effect of short-range order on structural behavior

Short-range order describes nearest-neighbor correlations between cation site occupancies, i.e., how the occupancy of one site is influenced by the occupancy of its neighboring sites. For example, the probability of finding a Ti-Ti pair across the nearest-neighbor A-B join can be written:

$$P_{\mathrm{Ti-Ti}}^{\mathrm{A-B}} = X_{\mathrm{Ti}}^{\mathrm{A}} X_{\mathrm{Ti}}^{\mathrm{B}}(1-\sigma) \quad (4)$$

where σ is the short-range order parameter (Vinograd et al. 1997). When $\sigma = 0$ (no short-range order) $P_{\mathrm{Ti-Ti}}^{\mathrm{A-B}}$ is equal to the product of the point probabilities of finding Ti on the A- and B-sites. The point probabilities are a simple function of the bulk composition and the degree of long-range order (Eq. 1). When $\sigma = 1$ (full short-range order) the probability of finding Ti on A next to Ti on B is zero. Similar definitions describe avoidance of Fe-Ti intralayer cation pairs.

Short-range order becomes important at temperatures close-to and above T_c, where Fe and Ti mix on both the A- and B-layers. In addition, one expects that short-range ordering above T_c will be more important at compositions close to ilm100, where the Fe:Ti ratio approaches 1:1. Long and short-range parameters in Figure 8 were calculated as a function of temperature assuming Ising-like behavior and an Fe:Ti ratio of 1:1. The rapid increase in the degree of short-range order at temperatures

approaching T_c correlates with the rapid decrease in long-range order. Above T_c, σ decreases slowly, driven by the increase in configurational entropy at higher temperatures.

Earlier we concluded that the spontaneous strain for long-range ordering was approximately a pure shear (with e_{11} and e_{33} having opposite sign and $e_v \approx 0$) and the spontaneous strain for short-range ordering was a volume strain (with e_{11} and e_{33} having the same sign and $e_v \neq 0$). For the *a* cell parameter, the strains due to decreasing *Q* and increasing σ compensate for each other as the transition temperature is approached. This leads to a rather smooth variation in *a* as function of *T*, with no sharp change in *a* at $T = T_c$ (Fig. 8b). For the *c* cell parameter, the two strain components reinforce each other, leading to a large and abrupt change in *c* at $T = T_c$ (Fig. 3). According to the arguments above, one expects this effect to be more obvious for bulk compositions close to ilm100, as seen in Figure 3.

Similar arguments explain the temperature-dependence of the cation-cation distances (Fig. 4). The phase transition in ilm90 is accompanied by a large and rapid increase in both the A-B and B-B distances (Figs. 4a and 4c). These changes correspond to an increase in the degree of distortion of the puckered hexagonal rings which form the (001) B-cation layer (Fig. 1). In comparison, the increase in A-A distance occurs smoothly (Fig. 4b). The two factors which determine the degree of distortion of the (001) cation layers are the total concentration of Ti in the layer (which is a function of *Q*) and the degree of short-range order within the layer (which is a function of σ). A high concentration of Ti in the layer correlates with a low degree of distortion, which accounts for the small A-B and B-B distances in ordered ilm90. A high degree of intralayer short-range order correlates with a high degree of distortion, accounting for the large A-B and B-B distances in disordered ilm90. As the sample disorders, the concentration of Ti on the B-layer decreases and therefore the degree of distortion increases. Simultaneously the degree of short-range order within the B-layers increases, further enhancing the distortion. These two effects reinforce each other, leading to a large and rapid change in A-B and B-B distances at the transition temperature. The opposite is true for the A-layer, where the effect of increasing the A-layer Ti concentration on disordering is counteracted by the effect of increasing the degree of short-range order.

The cation-cation distances in ilm70 appear to be different to those in ilm90. The behavior below 600 °C is strongly influenced by the effects of exsolution. However, the trend of decreasing A-B and B-B distances between 600 and 1000 °C must be explained in terms of homogeneous material, because these temperatures lie above the solvus. From the arguments presented above, one concludes that the unusually large A-B and B-B distances observed in ilm70 at 600 °C are caused by a significant distortion of the hexagonal rings in the B-layer. This distortion has two origins. First, the Ti concentration in the B-layer is relatively low (around 64%, compared with 89% for ilm90 at 600 °C). Second, short-range chemical heterogeneities are likely to be present at temperatures just above the solvus, which may result in local strains and a further distortion of the B-layer. The trend of decreasing A-B and B-B distances with increasing temperature could then be explained if the effect of decreasing the concentration of Ti on the B-layer on disordering is outweighed by the effect of homogenizing the sample at temperatures far above the solvus. Although such an explanation is consistent with the observed structural changes, it remains speculative in the absence of more direct information about the short-range structure in this material.

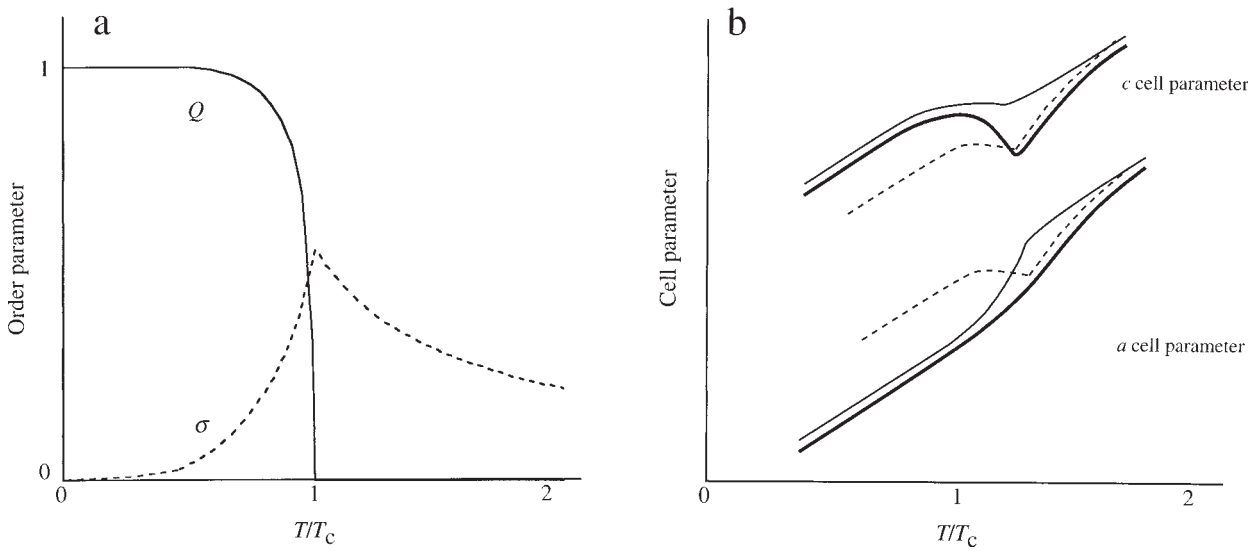

FIGURE 8. (**a**) Schematic variation in long-range order parameter, *Q*, and short-range order parameter, σ, as a function of temperature. (**b**) Effect of competing long- and short-range order on the lattice parameters *a* and *c* as a function of temperature. Thin solid lines show the effect of long-range ordering only, dashed lines show the effect of short-range ordering. The thick solid lines show the sum of long-range and short-range effects.

ACKNOWLEDGMENTS

The authors thank V. Vinograd for his help in preparing Figure 8a. R.J.H. acknowledges the support of the Marie Curie Fellowship.

REFERENCES CITED

Banerjee, S.K. (1991) Magnetic properties of Fe-Ti oxides. In Mineralogical Society of America Reviews in Mineralogy, 25, 107–128.

Brown, N.E., Navrotsky, A., Nord, G.L., and Banerjee, S.K. (1993) Hematite (Fe_2O_3)-Ilmenite ($FeTiO_3$) solid solutions: Determinations of Fe-Ti order from magnetic properties. American Mineralogist, 78, 941–951.

Buddington, A.F. and Lindsley, D.H. (1964) Iron-titanium oxide minerals and synthetic equilivalents. Journal of Petrology, 5, 310–357.

Burton, B. (1984) Thermodynamic analysis of the system Fe_2O_3-$FeTiO_3$. Physics and Chemistry of Minerals, 11, 132–139.

——(1985) Theoretical analysis of chemical and magnetic ordering in the system Fe_2O_3-$FeTiO_3$. Americal Mineralogist, 72, 329–336.

Carpenter, M.A., Salje, E.K.H., and Graeme-Barber, A. (1998) Spontaneous strain as a determinant of thermodynamic properties for phase transitions in minerals. European Journal of Mineralogy, 10, 621–691.

Deines, P., Nafziger, R.H., Ulmer, G.C., and Woermann, E. (1974) Temperature-oxygen fugacity tables for selected gas mixtures in the system C-H-O at one atmosphere total pressure. Pennsylvania State University, College of Earth and Mineral Sciences, Bulletin of the experimental station, 88, 129.

Ghiorso, M.S. (1990) Thermodynamic properties of hematite-ilmenite-geikielite solid solution. Contributions to Mineralogy and Petrology, 104, 645–667.

——(1997) Thermodynamic analysis of the effect of magnetic ordering on miscibility gaps in the FeTi cubic and rhombohedral oxide minerals and the FeTi oxide geothermometer. Physics and Chemistry of Minerals, 25, 28–38.

Grguric, B.A., Putnis, A., and Harrison, R.J. (1999) An investigation of the phase transitions in bornite (Cu_5FeS_4) using neutron diffraction and differential scanning calorimetry. American Mineralogist, 83, 1231–1239.

Harrison, R.J., Dove, M.T.D., Knight, K.S., and Putnis, A. (1999) In situ neutron diffraction study of non-convergent ordering in the spinel solid solution $(Fe_3O_4)_{1-x}(MgAl_2O_4)_x$: kinetics and equilibrium ordering. American Mineralogist, 84, 555–563.

Harrison, R.J., Redfern, S.A.T., and O'Neill, H.S.C. (1998) The temperature dependence of the cation distribution in synthetic hercynite ($FeAl_2O_4$) from in-situ neutron diffraction. American Mineralogist, 83, 1092–1099.

Holland, T.J.B. and Redfern, S.A.T. (1997) Unit cell refinement from powder diffraction data: The use of regression diagnostics. Mineralogical Magazine, 61, 65–77.

Ishikawa, Y. (1958) An order-disorder transformation phenomenon in the $FeTiO_3$-Fe_2O_3 solid solution series. Journal of the Physical Society of Japan, 13, 828–837.

——(1962) Magnetic properties of the ilmenite-hematite system at low temperature. Journal of the Physical Society of Japan, 17, 1835–1844.

Ishikawa, Y. and Akimoto, S. (1957) Magnetic properties of the $FeTiO_3$–Fe_2O_3 solid solution series. Journal of the Physical Society of Japan, 12, 1083–1098.

Ishikawa, Y. and Syono, Y. (1963) Order-disorder transformation and reverse thermoremanent magnetization in the $FeTiO_3$-Fe_2O_3 system. Journal of the Physics and Chemistry of Solids, 24, 517–528.

Kikuchi, R. (1951) A theory of cooperative phenomena. The Physical Review, 81, 988–1003.

Larson, A.C. and Von Dreele, R.B. (1994) GSAS general structure analysis system. In: LANSCE MS-H805. Los Alamos National Laboratory.

Lindsley, D.H. (1965) Iron-titanium oxides. Carnegie Institution of Washington Yearbook, 64, 144–148.

Nafziger, R.H., Ulmer, G.C., and Woermann, E. (1971) Gaseous buffering for the control of oxygen fugacity at one atmosphere pressure. In: G. C. Ulmer (ed.) Research techniques for high pressure and high temperature. Springer-Verlag, New York.

Nord, G.L. and Lawson, C.A. (1989) Order-disorder transition-induced twin domains and magnetic properties in ilmenite-hematite. American Mineralogist, 74, 160.

——(1992) Magnetic properties of ilmenite70-hematite30: effect of transformation-induced twin boundaries. Journal of Geophysical Research, 97B, 10897.

Redfern, S.A.T., Henderson, C.M.B., Wood, B.J., Harrison, R.J., and Knight, K.S. (1996) Determination of olivine cooling rates from metal-cation ordering. Nature, 381, 407–409.

Redfern, S.A.T., Harrison, R.J., O'Neill, H.S.C., and Wood, D.R.R. (1999) Thermodynamics and kinetics of cation ordering in $MgAl_2O_4$ spinel up to 1600 °C from in situ neutron diffraction. American Mineralogist, 84, 299–310.

Ross, C.R. (1991) Ising models and geological applications. In J. Ganguly, Ed., Diffusion, atomic ordering and mass transport: Selcted topics in geochemistry. Springer-Verlag, New York.

Shirane, G., Cox, D.E., Takei, W.J., and Ruby, S.L. (1962) A study of the magnetic properties of the $FeTiO_3$-Fe_2O_3 system by neutron diffraction and the Mössbauer effect. Journal of the Physical Society of Japan, 17, 1598–1611.

Shirane, G., Pickart, S.J., Nathans, R., and Ishikawa, Y. (1959) Neutron-diffraction study of antiferro-magnetic $FeTiO_3$ and its solid solutions with α-Fe_2O_3. Journal of Physics and Chemistry of Solids, 10, 35–43.

Vinograd, V., Saxena, S.K., and Putnis, A. (1997) Calculation of the probability distribution of basic clusters involved in cluster-variation approximations to the Ising model. Physical Review B, 56, 11493–11502.

Warner, B.N., Shive, P.N., Allen, J.L., and Terry, C. (1972) A study of the hematite-ilmenite series by the Mössbauer effect. Journal of Geomagnetism and Geoelectricity, 24, 353–367.

Waychunas, G.A. (1991) Crystal chemistry of oxides and oxyhydroxides. In Mineralogical Society of America Reviews in Mineralogy, 25, 11–68.

Wechsler, B.A. and Prewitt, C.T. (1984) Crystal structure of ilmenite ($FeTiO_3$) at high temperature and at high pressure. American Mineralogist, 69, 176–185.

MANUSCRIPT RECEIVED APRIL 19, 1999
MANUSCRIPT ACCEPTED SEPTEMBER 15, 1999
PAPER HANDLED BY BRYAN CHAKOUMAKOS